Core-hole-electron interaction in x-ray Raman scattering

2001 J. Phys.: Condens. Matter 13 8039

(http://iopscience.iop.org/0953-8984/13/35/311)

INSTITUTE OF PHYSICS PUBLISHING JOURNAL OF PHYSICS: CONDENSED MATTER

J. Phys.: Condens. Matter **13** (2001) 8039–8047 PII: S0953-8984(01)25107-8

Core-hole–electron interaction in x-ray Raman scattering

J A Soininen[1], K Hämäläinen[1], W A Caliebe[2], C-C Kao[2] and Eric L Shirley[3]

[1] Department of Physics, POB 64, FIN-00014, University of Helsinki, Finland
[2] National Synchrotron Light Source, Brookhaven National Laboratory, Upton, NY 11973, USA
[3] Optical Technology Division, Physics Laboratory,
National Institute of Standards and Technology, Gaithersburg, Maryland 20899, USA

Received 21 May 2001
Published 16 August 2001
Online at stacks.iop.org/JPhysCM/13/8039

Abstract

This work applies a recently developed *first-principles* scheme for calculating core excited states in solids to non-resonant inelastic x-ray scattering. The model explicitly includes the interaction between the excited electron and the core hole. The calculated results are compared with recent experimental results on inelastic x-ray scattering from K shells of Li, Be and C in lithium fluoride, beryllium oxide and diamond, respectively. The overall agreement between experimental and theoretical spectra is found to be good in all cases, even for the near-edge structure.

1. Introduction

It is well known that inelastic scattering probes, such as non-resonant inelastic x-ray scattering (NRIXS) and electron-energy-loss spectroscopy (EELS), can provide similar information to optical or x-ray absorption spectroscopy (XAS). Additional information in NRIXS and EELS as a function of energy loss can be obtained by varying the magnitude and the direction of the momentum transfer probed. This can be used, for example, to study the dispersion of longitudinal excitons in insulators [1, 2], the spatial dimensions of excitons in molecular systems [3] and the directional dependences of plasmon dispersions in semiconductors [4, 5] and metals [6, 7]. The momentum-transfer dependence of x-ray edges has also been studied using NRIXS [8].

Our analysis uses a recently developed *first-principles* scheme for modelling inner-shell excitations created by inelastic scattering. Here we compare calculated results to recent experimental x-ray Raman scattering data for K edges that can be quite different in character. X-ray Raman spectra for the Be K edge in BeO show a strongly bound core exciton that gives rise to a pronounced, well-separated peak in the experimental data. The Li K edge in LiF, on the other hand, shows two strongly bound exciton levels with different symmetries (even and

odd parity), whose spectral weights vary as a function of momentum transfer. We have also studied the carbon K-edge fine structure in diamond, which has attracted substantial interest over the years and is known to have a weakly bound core exciton.

An accurate theoretical treatment of inelastic scattering requires going beyond a simple single-particle picture. In this work, we treat the scattering process as a two-body problem (one electron plus one hole). This is done by solving the Bethe–Salpeter equation (BSE), i.e., the equation of motion of the two-body Green's function [9, 10]. In recent years there have been several studies applying this formalism at an *ab initio* level to optical absorption [11–13], and also very recently to NRIXS from valence electrons of semiconductors [1].

We wish to emphasize the need to include the core-hole–electron interaction in the description of x-ray Raman scattering (XRS). We have used a *first-principles* scheme [14] to model the core-hole potential that the excited electron experiences in the final state. The edge region of the spectra is most sensitive to the core-hole potential. Further away from the edge, the crystal potential of the material becomes more important. Both of these regions of the spectra can be studied with non-resonant inelastic x-ray scattering, but here we concentrate on the near-edge structure.

We first introduce the relation between the double-differential scattering cross section measured in NRIXS investigations and the dynamic structure factor describing the target system's macroscopic response to an external electromagnetic field. Next, we discuss the implementation of the computational scheme for XRS studies. A short description of the experimental set-up is also given. Finally, we compare and analyse the differences between calculated and experimental spectra.

2. X-ray Raman scattering

Within first-order perturbation theory the double-differential scattering cross section for inelastic x-ray scattering can be written with the help of the dynamic structure factor, $S(\boldsymbol{q}, \omega)$:

$$\frac{\mathrm{d}^2\sigma}{\mathrm{d}\Omega\,\mathrm{d}\omega} = (\mathrm{d}\sigma/\mathrm{d}\Omega)_{Th} S(\boldsymbol{q}, \omega)$$

where $(\mathrm{d}\sigma/\mathrm{d}\Omega)_{Th}$ is the Thomson scattering cross section. $S(\boldsymbol{q}, \omega)$ depends only on the momentum $\boldsymbol{q}$ and energy ω transferred from the photon to the scattering system. The dynamic structure factor can be written in terms of the initial ($|I\rangle$) and the final ($|F\rangle$) electron states as

$$S(\boldsymbol{q}, \omega) = \sum_F |\langle F| \sum_i \mathrm{e}^{\mathrm{i}\boldsymbol{q}\cdot\boldsymbol{r}_i} |I\rangle|^2 \delta(\omega + E_I - E_F)$$

where E_I is the initial- and E_F the final-state energy. The index i runs over all electrons. Using the completeness of the final states and taking the ground state $|0\rangle$ as the initial state we can rearrange the expression for $S(\boldsymbol{q}, \omega)$ as

$$S(\boldsymbol{q}, \omega) = \lim_{\eta \to 0} \left[-\frac{1}{\pi} \mathrm{Im} \langle 0| \hat{\rho}_{\boldsymbol{q}} \frac{1}{\omega - \hat{H} + \mathrm{i}\eta} \hat{\rho}_{\boldsymbol{q}}^{\dagger} |0\rangle \right]. \tag{1}$$

$\hat{H}$ is the Hamiltonian of the system and $\hat{\rho}_{\boldsymbol{q}}$ is a Fourier component of the density operator. In the second-quantized form, $\hat{\rho}_{\boldsymbol{q}}$ is

$$\hat{\rho}_{\boldsymbol{q}}^{\dagger} = \sum_{i,j,\boldsymbol{k},\boldsymbol{k}'} \langle \psi_{i\boldsymbol{k}} | \mathrm{e}^{\mathrm{i}\boldsymbol{q}\cdot\boldsymbol{r}} | \psi_{j\boldsymbol{k}'} \rangle \hat{a}_{i\boldsymbol{k}}^{\dagger} \hat{a}_{j\boldsymbol{k}'} \tag{2}$$

where $\psi_{i\boldsymbol{k}}$ and $\psi_{j\boldsymbol{k}'}$ are unoccupied and occupied single-particle states, respectively. When the occupied state in equation (2) is a localized core state, and the momentum transfer is small, the dipole approximation $\mathrm{e}^{\mathrm{i}\boldsymbol{q}\cdot\boldsymbol{r}} \approx 1 + \mathrm{i}\boldsymbol{q}\cdot\boldsymbol{r}$ is valid. In this case $\hat{\rho}_{\boldsymbol{q}}$ reduces to a dipole operator and

$S(\boldsymbol{q}, \omega)$ for XRS has an expression that is equivalent to the cross section for x-ray absorption, except that the polarization vector is replaced by the momentum-transfer vector [15]. When the momentum transfer is increased, the dipole approximation is no longer valid and excitations with different spatial symmetries can be studied.

As explained in reference [14], we approximate the core-excited-state wave function with an electron–core-hole pair wave function:

$$\Phi(\boldsymbol{r}_e, \boldsymbol{r}_h) = \sum_{n\boldsymbol{k}} C_{n\boldsymbol{k}} \psi_{n\boldsymbol{k}}(\boldsymbol{r}_e) \left[\psi^{TB}_{\boldsymbol{k}-\boldsymbol{q}\alpha}(\boldsymbol{r}_h)\right]^*$$

where $\psi_{n\boldsymbol{k}}$ is a conduction band state, $\psi^{TB}_{\boldsymbol{k}-\boldsymbol{q}\alpha}$ is a tight-binding core state and $C_{n\boldsymbol{k}}$ are the expansion coefficients. The atomic state nlm of the core hole and its position in the unit cell $\boldsymbol{\tau}$ are represented by the parameter α:

$$\psi^{TB}_{\boldsymbol{k}-\boldsymbol{q}\alpha}(\boldsymbol{r}_h) = (1/\sqrt{N}) \sum_{\boldsymbol{R}} \mathrm{e}^{\mathrm{i}(\boldsymbol{k}-\boldsymbol{q})\cdot(\boldsymbol{R}+\boldsymbol{\tau})} \phi_{nlm}(\boldsymbol{r}_h - \boldsymbol{R} - \boldsymbol{\tau})$$

where N is the number of $\boldsymbol{k}$-points. The summation is done over the lattice vectors $\boldsymbol{R}$ and the basis vector τ has a single value. In what follows, we will denote the electron–core-hole pair wave function with the appropriate indices as $\psi_{n\boldsymbol{k}}(\boldsymbol{r}_e)[\psi^{TB}_{\boldsymbol{k}-\boldsymbol{q}\alpha}(\boldsymbol{r}_h)]^* \doteq |n\boldsymbol{k}\alpha\rangle$. The conduction band wave functions $\psi_{n\boldsymbol{k}}$ are calculated using local-density-approximation (LDA) [16] pseudopotential [17] codes and the atomic wave functions ϕ_{nlm} used for the core hole are calculated with an atomic, Hartree–Fock code. As an approximation for the full many-body Hamiltonian $\hat{H}$ in equation (1) we use an effective Hamiltonian:

$$\hat{H}_{eff} = \hat{H}_0 + \hat{V}_D + \hat{V}_X.$$

The effective Hamiltonian includes a single-particle part, $\hat{H}_0$, and direct ($\hat{V}_D$) and exchange ($\hat{V}_X$) interactions of the electron with the core hole. The matrix elements of $\hat{H}_{eff}$ are

$$\langle n\boldsymbol{k}\alpha|\hat{H}_{eff}|n'\boldsymbol{k}'\alpha'\rangle = \delta_{\alpha\alpha'}[(\varepsilon_{n\boldsymbol{k}} - E_\alpha)\delta_{nn'}\delta_{\boldsymbol{k}\boldsymbol{k}'} + \langle\psi_{n\boldsymbol{k}}|\hat{V}_D(\alpha) + \hat{V}_X(\alpha)|\psi_{n'\boldsymbol{k}'}\rangle].$$

Here $\varepsilon_{n\boldsymbol{k}}$ is the single-particle energy of the conduction band electron and E_α is the core-hole energy. In our current scheme the core-hole energy is not calculated and E_α is set equal to the conduction band minimum (CBM). When comparing calculated spectra with the experimental results, a rigid shift in energy is applied to the calculated spectrum to put it on the same energy scale as the experimental one. Because the core-hole state is kept fixed in the calculation, the electron–core-hole interaction effectively couples different electron states. This means that the final-state electron feels an effective, symmetry-broken, single-particle potential. As explained in [14] we separate V_D into three parts:

$$V_D(\boldsymbol{r}) = V_\alpha(\boldsymbol{r}) + \Delta V_\alpha(\boldsymbol{r}) + \Delta V_{val}(\boldsymbol{r}). \tag{3}$$

Here V_α is the bare core-hole potential, $\Delta V_\alpha(\boldsymbol{r})$ accounts for screening by the core electrons and $\Delta V_{val}(\boldsymbol{r})$ accounts for screening by the valence electrons. The first two terms $V_\alpha(\boldsymbol{r}) + \Delta V_\alpha(\boldsymbol{r})$ are calculated within an atomic program. The valence screening is calculated using a RPA [18] dielectric matrix ε^{-1}:

$$\Delta V_{val}(\boldsymbol{r}) = \int \mathrm{d}^3 r' \, (\varepsilon^{-1}(\boldsymbol{r}, \boldsymbol{r}') - \delta(\boldsymbol{r} - \boldsymbol{r}'))(V_\alpha(\boldsymbol{r}') + \Delta V_\alpha(\boldsymbol{r}')).$$

A similar approach was applied to screening of impurities by Mattausch *et al* [19]. In principle, the screening potential should be energy dependent as explained in references [10] and [20]. However, this energy dependence would make the Hamiltonian non-Hermitian, which would increase the computational cost considerably. The potential V_D has the correct long-range behaviour, $1/(\varepsilon_\infty r)$, where ε_∞ is the macroscopic dielectric constant. Matrix elements involving the core and conduction band states are needed for computing the exchange potential

V_X and $\hat{\rho}_q$. These matrix elements are calculated using a pseudopotential-inversion scheme that was originally developed in reference [21] and later refined [22].

Using the approximations introduced in this section, we can calculate the dynamic structure factor:

$$S(\boldsymbol{q},\omega) = -(1/\pi)\mathrm{Im}\sum_{n\boldsymbol{k}}\sum_{n'\boldsymbol{k}'}\langle 0|\hat{\rho}_{\boldsymbol{q}}|n\boldsymbol{k}\alpha\rangle\langle n\boldsymbol{k}\alpha|(\omega - \hat{H}_{eff} + \mathrm{i}\eta)^{-1}|n'\boldsymbol{k}'\alpha\rangle\langle n'\boldsymbol{k}'\alpha|\hat{\rho}_{\boldsymbol{q}}^{\dagger}|0\rangle$$

using the Haydock recursion method [23]. The broadening parameter η should include both electron and hole lifetime effects. We calculate the lifetime of the excited electron within the so-called 'GW approximation' [24], using a generalized plasmon-pole model and a model dielectric function [25]. This means that η depends on the excitation energy, and this dependence is easily realized by varying η when evaluating the continued-fraction expansion encountered at the end of one calculation when using the Haydock recursion method. (The 'GW approximation' derives its name from its approximating the electron self-energy as the product of the one-electron Green's function G and the dynamically screening Coulomb interaction W.)

3. Experimental set-up

The scattering experiments reported here were carried out at the inelastic scattering beamline X21 at the National Synchrotron Light Source (USA). The radiation from the multipole wiggler was monochromatized using a horizontally bent triangular silicon (220) crystal. The Rowland circle geometry produced simultaneous focusing to the sample with a spot size of 0.2 mm horizontal $\times$ 10 mm vertical and a monochromatic flux of about 2×10^{11} photons s^{-1}. The scattered photon energy was analysed utilizing a Rowland circle spectrometer with a spherically bent silicon (111) analyser crystal with bending radius of 1 m. During energy-loss scans, the analyser Bragg angle was kept fixed within a few degrees off of the backscattering geometry to minimize the source-size contribution to the energy resolution, while the incident energy was scanned over the desired range. The incident flux was monitored by an ion chamber. The total-energy resolution (determined from the width of the quasielastic line) varied, depending on the sample, between 0.7 eV and 1 eV. The experimental set-up is described in more detail elsewhere [26, 27]. All the measurements were carried out either in symmetric reflection or symmetric transmission geometries with the momentum transfer perpendicular or parallel to the sample surface, respectively. The momentum transfer was controlled by varying the scattering angle. Single crystals of diamond and LiF were used, while the BeO was polycrystalline.

4. Results and discussion

The experimental XRS results for near the Be K edge in BeO can be seen in figure 1, together with our calculations with and without the core-hole–electron interaction. Because a polycrystalline BeO sample was used in the experiment, the calculations required a spherical average to be taken over the direction of momentum transfers using a six-point formula [28] for the integration. For the calculations, we have used lattice constants $a = 2.698$ Å, $c = 4.380$ Å and the wurtzite structure with internal parameter $u = 0.378$ to calculate LDA band energies and the wave functions. Our calculated conduction bandwidth was increased by 11% to agree with GW [24] band energies. A linear background arising from scattering from the valence electrons was subtracted from the experimental data, which were then normalized to have the same area under the curve as the calculated spectra for the energy range shown in the figure. The most pronounced feature of the experimental spectrum is the strong core-exciton peak

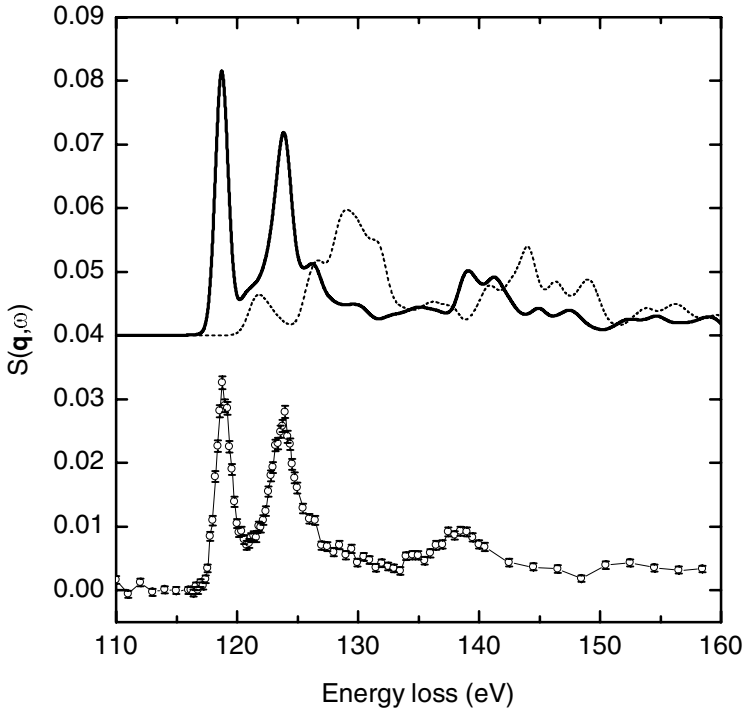

Figure 1. Calculated and measured x-ray Raman scattering spectra at the Be K edge in BeO. The momentum transfer is 1.77 Å^{-1}. The error bars drawn for the experimental data points indicate the standard uncertainty. The calculated spectra (offset vertically) with and without the core-hole–electron interaction are given by the solid and dashed line, respectively.

around 119 eV that is about 0.74 eV below the edge of the conduction band. As expected, this peak is present in the spectrum calculated with the electron–core-hole interaction but absent in the spectrum that was calculated neglecting this interaction. The overall spectral features in the experimental spectra and spectra calculated including the core-hole–electron interaction show good agreement up to quite large energy transfers. However, the calculation slightly overestimates the spectral weight of the core exciton. On the other hand, the near-edge structure and overall agreement are completely lost if the interaction is neglected.

The double-peak exciton structure at the Li K edge in LiF has been previously studied with EELS [2] and serves as another good example to use to study the validity of our experimental technique and the computational scheme. LiF has the rock-salt structure with a lattice constant of 4.02 Å. Figure 2 shows the experimental result for the dynamic structure factor $S(\boldsymbol{q}, \omega)$ extracted from the inelastic scattering cross section for three momentum transfers along the Cartesian (100) direction. The calculated spectra for the same momentum-transfer values are shown in figure 3. Both the experimental and the calculated results show two distinct exciton peaks about 3 eV below the continuum edge (around $\omega = 64.5$ eV).

On the basis of the calculations, the two peaks in the experimental spectra can be associated with the even-parity (dipole-forbidden) exciton around 61.5 eV and the odd-parity (dipole-allowed) exciton around 62.2 eV. For the low-momentum region, the dipole-allowed transition is dominant, but as the momentum transfer is increased, the weight of the even-parity exciton increases. This characteristic can be qualitatively explained by the behaviour of the corresponding matrix elements.

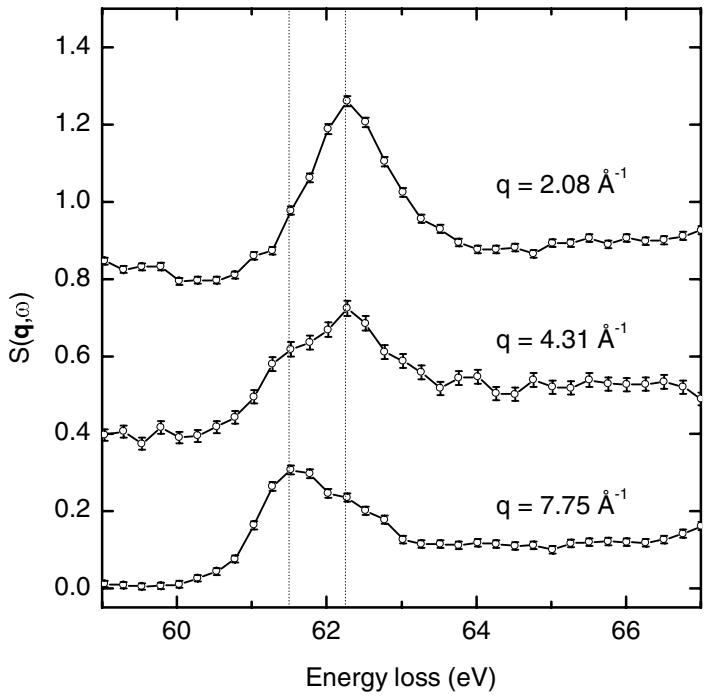

Figure 2. Experimental spectra at the Li K edge in LiF. The magnitudes of the momentum transfers are given in the figure. The error bars drawn for the experimental data points indicate the standard uncertainty. The spectra are offset for clarity and scaled to have approximately the same peak height. The estimated positions of the even- and odd-parity excitons are indicated by the dashed vertical lines.

The intensity variation of the exciton peaks of the calculated spectra follows quite faithfully the behaviour found in the experimental spectra, although the energy splitting between the even- and odd-parity excitons is underestimated. Because the calculated splitting is too small, the spectra calculated using the experimental resolution of 0.7 eV do not show the same shoulder structure as the experimental spectra. However, this structure is clearly visible if a better resolution of 0.2 eV is used. We speculate that the predicted splitting is too small because we fail to include correlation between the excited electron and the remaining Li 1s core electron. In the free Li^+ ion, the $1s^12s^1(^1S) \rightarrow 1s^12p^1(^1P)$ splitting is 1.29 eV, compared to 0.98 eV as found in a Hartree–Fock calculation (with proper symmetrization of the spatial part of the wave function in the singlet state taken into account). Presumably, an analogous underestimation of the splitting in our present solid-state calculation should also arise. Results for the calculations that neglect the electron–core-hole interaction are not shown, because they do not treat the excitons at all.

As our last example, we consider the near-edge structure of diamond, which has attracted experimental and theoretical interest [29–31]. We have calculated the single-particle states and energies for diamond within the LDA using a lattice constant of 3.57 Å. The calculated and the experimental results for the structure near the C K edge for diamond in XRS are shown in figure 4. The energy scale of the calculated spectra is shifted by 290 eV. The calculated results with and without including the electron–core-hole interaction are shown, and experimental spectra were normalized in the same way as for BeO. The spectrum calculated including the interaction correctly predicts the weight and shape of most of the various structures observed

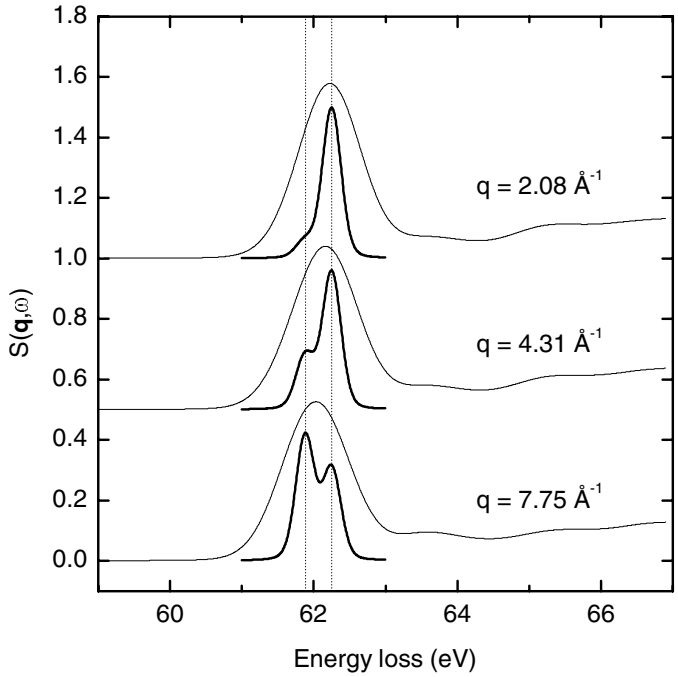

Figure 3. Calculated spectra at the Li K edge in LiF. The magnitudes of the momentum transfers are given in the figure. For each value of momentum transfer two calculated curves are given. The thin solid line is calculated using the experimental energy resolution of 0.7 eV. The bold solid line is calculated using a smaller (0.2 eV) resolution in order to separate the even- and odd-parity exciton lines. The calculated positions of the even- and odd-parity excitons are indicated by the dashed vertical lines. The data are offset and scaled as in figure 2.

in the spectrum. The structure at the edge, which can be attributed to the previously mentioned shallow core exciton, is overestimated. Additionally, the features around 297 eV and 306 eV are shifted down by about 1 eV in the calculated spectra. This seems to indicate that the core-hole–electron interaction is slightly overestimated in the current scheme. However, the disagreement between the calculated and experimental spectra is much worse if the interaction is totally neglected. The 290 eV shift used for diamond is slightly higher than the continuum edge estimated by other experimental methods (Ma *et al*: 289.7 eV [29]; Morar *et al*: 289.2 eV [29]; and Batson *et al*: 289.18 eV [30]). However, it gives reasonable agreement between the theoretical and experimental XRS edge positions when the overestimation of the exciton effects is taken into account.

5. Conclusions

We have presented theoretical and experimental results for non-resonant x-ray Raman scattering from core electrons in several different materials: Li 1s electrons in LiF, Be 1s electrons in BeO and C 1s electrons in diamond. The overall agreement between the experimental and the calculated results is very good, with spectral features near the edge being rather well reproduced. As an exception, the theoretical splitting of the double-peak exciton structure at the Li K edge in LiF was too small, which we suggest could result from neglecting correlation effects involving the exciton's electron and the remaining Li 1s core electron.

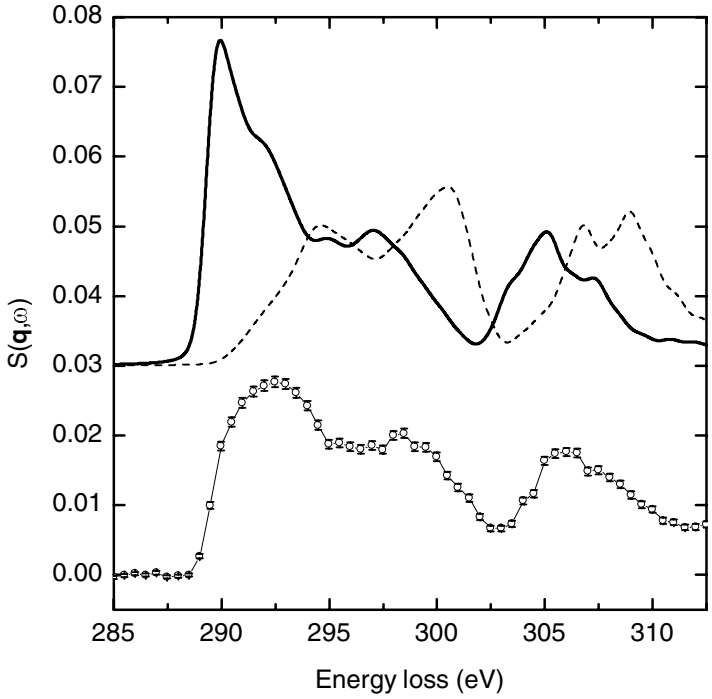

Figure 4. Calculated x-ray Raman spectra near the C K edge in diamond together with a measured excitation spectrum. The momentum transfer is 2.74 $Å^{-1}$ along the [111] direction. Calculated results including the core-hole–electron interaction are indicated by the solid line, whereas the dashed line indicates results that omit the interaction. The calculated spectra are offset for clarity.

Otherwise positions of the excitations seem to be rather well predicted using our current scheme. Examined more closely, the relative weight of the near-edge structures is sometimes slightly wrong. One possible reason for this is the fact that even a small error in the core-hole potential can have a large effect on these features.

In conclusion, this work gives examples of the ability to vary the momentum transfer in the case of non-resonant inelastic x-ray scattering. This makes such scattering a complementary way to study features close to the edges from a momentum viewpoint and, in particular, to examine transitions that are not dipole allowed. Furthermore, for the cases considered in the work, most spectral features are qualitatively and even quantitatively well understood on the basis of first-principles calculations.

Acknowledgments

This project was supported by the Academy of Finland (7379/39182/40732) and the US Department Energy (W-31-109-ENG-38).

References

[1] Caliebe W A, Soininen J A, Shirley E L, Kao C-C and Hämäläinen K 2000 *Phys. Rev. Lett.* **84** 3907
Soininen J A and Shirley E L 2000 *Phys. Rev.* B **61** 16 423
[2] Fields J R, Gibbons P C and Schnatterly S E 1977 *Phys. Rev. Lett.* **38** 430

[3] Knupfer M, Pichler T, Golden M S, Fink J, Murgia M, Michel R H, Zamboni R and Taliani C 1999 *Phys. Rev. Lett.* **83** 1443
[4] Schülke W, Schmitz J R, Schulte-Schrepping H and Kaprolat A 1995 *Phys. Rev.* B **52** 11 721
[5] Waidmann S, Knupfer M, Arnold B and Fink J 2000 *Phys. Rev.* B **61** 10 149
[6] Hill J P, Kao C-C, Caliebe W A, Gibbs D and Hastings J B 1996 *Phys. Rev. Lett.* **77** 3665
[7] vom Felde A, Sprösser-Prou J and Fink J 1989 *Phys. Rev.* B **40** 10 181
[8] Krisch M H, Sette F, Masciovecchio C and Verbeni R 1997 *Phys. Rev. Lett.* **78** 2843
Nagasawa H, Mourikis S and Schülke W 1988 *J. Phys. Soc. Japan* **58** 710
[9] Sham L J and Rice T M 1966 *Phys. Rev.* **144** 708
[10] Strinati G 1984 *Phys. Rev.* B **29** 5718
[11] Benedict L X and Shirley E L 1999 *Phys. Rev.* B **59** 5441
Benedict L X, Shirley E L and Bohn R B 1998 *Phys. Rev.* B **57** 9385
Benedict L X, Shirley E L and Bohn R B 1998 *Phys. Rev. Lett.* **80** 4514
[12] Rohlfing M and Louie S G 1998 *Phys. Rev. Lett.* **80** 3320
Rohlfing M and Louie S G 1998 *Phys. Rev. Lett.* **81** 2312
[13] Albrecht S, Reining L, Del Sole R and Onida G 1998 *Phys. Rev. Lett.* **80** 4510
[14] Soininen J A and Shirley E L 2001 *Phys. Rev.* B at press
[15] Mizuno Y and Ohmura Y 1967 *J. Phys. Soc. Japan* **22** 445
[16] Hohenberg P and Kohn W 1964 *Phys. Rev.* **136** 864
Kohn W and Sham L J 1965 *Phys. Rev.* **140** 1133
[17] For a review, see Pickett W E 1989 *Comput. Phys. Rep.* **9** 115
[18] Hybertsen M S and Louie S G 1987 *Phys. Rev.* B **35** 5585
[19] Mattausch H J, Hanke W and Strinati G 1983 *Phys. Rev.* B **27** 3735
[20] Rohlfing M and Louie S G 2000 *Phys. Rev.* B **62** 4927
[21] Shirley E L 2000 *J. Electron Spectrosc. Relat. Phenom.* **110–111** 305
[22] Shirley E L, Merritt S I and Soininen J A 2001 to be submitted
[23] Haydock R 1980 *Solid State Physics* vol 35, ed H Ehrenreich, F Seitz and D Turnbull (New York: Academic) p 215
[24] Hedin L 1965 *Phys. Rev.* **139** 796
[25] Levine Z H and Louie S G 1982 *Phys. Rev.* B **25** 6310
Hybertsen M S and Louie S G 1988 *Phys. Rev.* B **37** 2733
[26] Kao C-C, Hämäläinen K, Krisch M, Siddons D P, Oversluizen T and Hastings J B 1995 *Rev. Sci. Instrum.* **66** 1699
[27] Caliebe W A 1997 *PhD Thesis* University of Kiel
[28] *Handbook of Mathematical Functions* 1972 ed M Abramowitz and I A Stegun (New York: Dover)
[29] Morar J F, Himpsel F J, Hollinger G, Hughes G and Jordan J L 1985 *Phys. Rev. Lett.* **54** 1960
Ma Y, Skytt P, Wassdahl N, Glans P, Gluo J and Nordgren J 1993 *Phys. Rev. Lett.* **71** 3725
[30] Batson P E and Bruley J 1991 *Phys. Rev. Lett.* **67** 350
Batson P E 1993 *Phys. Rev. Lett.* **70** 1822
[31] Jackson K A and Pederson M R 1991 *Phys. Rev. Lett.* **67** 2521
Nithianandam J 1992 *Phys. Rev. Lett.* **69** 3108